

# Journal of Astronomical Telescopes, Instruments, and Systems

AstronomicalTelescopes.SPIEDigitalLibrary.org

## Automatic selection of correlated double sampling timing parameters

Daniel P. Weatherill  
Ian Shipsey  
Kirk Arndt  
Richard Plackett  
Daniel Wood  
Kaloyan Metodiev  
Maria Mironova  
Daniela Bortoletto  
Nicolas Demetriou

**SPIE.**

Daniel P. Weatherill, Ian Shipsey, Kirk Arndt, Richard Plackett, Daniel Wood, Kaloyan Metodiev, Maria Mironova, Daniela Bortoletto, Nicolas Demetriou, "Automatic selection of correlated double sampling timing parameters," *J. Astron. Telesc. Instrum. Syst.* **5**(4), 041502 (2019), doi: 10.1117/1.JATIS.5.4.041502.

# Automatic selection of correlated double sampling timing parameters

Daniel P. Weatherill,<sup>\*</sup> Ian Shipsey, Kirk Arndt, Richard Plackett, Daniel Wood, Kaloyan Metodiev, Maria Mironova, Daniela Bortoletto, and Nicolas Demetriou  
University of Oxford, Department of Physics, Oxford, United Kingdom

**Abstract.** Correlated double sampling (CDS) is a process used in many charge-coupled device readout systems to cancel the reset noise component that would otherwise dominate. CDS processing typically consists of subtracting the integrated video signal during a “signal” period from that during a “reset” period. The response of this processing depends, therefore, on the shape of the video signal with respect to the integration bounds. In particular, the amount of noise appearing in the final image and the linearity of the pixel value with signal charge are affected by the choice of the CDS timing intervals. We use a digital CDS readout system which highly oversamples the video signal (as compared with the pixel rate) to reconstruct pixel values for different CDS timings using identical raw video signal data. We use this technique to develop insights into optimal strategy for selecting CDS timings both in the digital case (where the raw video signal may be available) and in the general case (where it is not). In particular, we show that the linearity of the CDS operation allows subtraction of the raw video signals of pixels in bias images from those in illuminated images to directly show the effects of CDS processing on the final (subtracted) pixel values. © 2019 Society of Photo-Optical Instrumentation Engineers (SPIE) [DOI: 10.1117/1.JATIS.5.4.041502]

Keywords: charge-coupled devices; correlated double sampling; readout electronics; astronomy.

Paper 19033SS received Apr. 15, 2019; accepted for publication Jul. 24, 2019; published online Aug. 22, 2019.

## 1 Introduction

Modern charge-coupled devices (CCDs) are capable of extremely low read noise which is crucial to the science goals of current and future astronomical observatories. For example, the baseline requirement of the sensors to be used in the Large Synoptic Survey Telescope (LSST) camera is a readout noise of  $5e^-$  rms equivalent at a pixel frequency of  $500 \text{ kpix s}^{-1}$ .<sup>1</sup> This requirement is driven by the need to maintain the instrumental readout noise below the sky background shot noise levels, in particular, in the short-wavelength u band.<sup>2</sup>

Typically, the dominant on-chip noise source of a CCD is the reset noise, which arises from the Johnson–Nyquist noise associated with the resetting of the sense node used to convert the accumulated charge into a voltage signal.<sup>3</sup> To achieve the best possible performance, this noise signal is typically removed via a process known as correlated double sampling (CDS). The remaining readout noise is then associated with thermal effects, carrier trapping, and semiconductor parameter variation within the amplification transistors (so-called “read noise”), which for a given bandwidth represents the lowest noise achievable using a conventional CCD output design. The CDS process can be implemented using various types of analog<sup>4</sup> or digital<sup>5</sup> methods, though in all cases the timing parameters of the CDS circuit operation must be correctly chosen to properly eliminate reset noise without introducing adverse artifacts into the measured pixel values in the form of structured noise patterns or excess nonlinearity.

In this paper, we present investigations into the effects of these timing parameters using a digital CDS system and an e2v

CCD250 sensor.<sup>6</sup> We perform analysis of the raw oversampled video data (before processing to produce pixel values) to find correct timing parameters for linearity and signal-to-noise ratio (SNR) using numerical optimization (see Sec. 5). Using the linearity property of the digital CDS operation, we also show that performing subtraction of the raw video signal for different pixels can give insight into the choice of timing parameters (see Sec. 6), a process which might usefully be implemented on any CDS system, even those without access to oversampled raw video data.

## 2 Correlated Double Sampling Background

A diagram of a typical CCD two-stage on-chip amplifier circuit is shown in Fig. 1. Reset noise is incurred in the readout process during the operation of the sense node reset transistor (labeled as Q1 in Fig. 1). When the reset signal  $\Phi_R$  is asserted, the voltage on the sense node is allowed to settle to the reset drain voltage  $V_{RD}$ . If the channel resistance of the reset transistor is  $R_{Q1}$ , there is a Johnson–Nyquist noise  $\sigma_{\text{rms}}$  on the voltage given by<sup>7</sup>

$$\sigma_{\text{rms}} = 2\sqrt{k_B T B R_{Q1}}, \quad (1)$$

where  $T$  is the temperature,  $k_B$  is the Boltzmann’s constant, and  $B$  is the bandwidth of the circuit. This bandwidth is set by the product of a resistance  $R$  and a capacitance  $C$  (RC) circuit formed by the finite channel resistance of the reset transistor  $R_{Q1}$  and the sense node capacitance  $C_N$ . Using the transfer function of an RC filter, we obtain the amount of noise present on the reset  $\sigma_{\text{rms}}$  expressed in units of electrons

<sup>\*</sup>Address all correspondence to Daniel P. Weatherill, E-mail: [daniel.weatherill@physics.ox.ac.uk](mailto:daniel.weatherill@physics.ox.ac.uk)

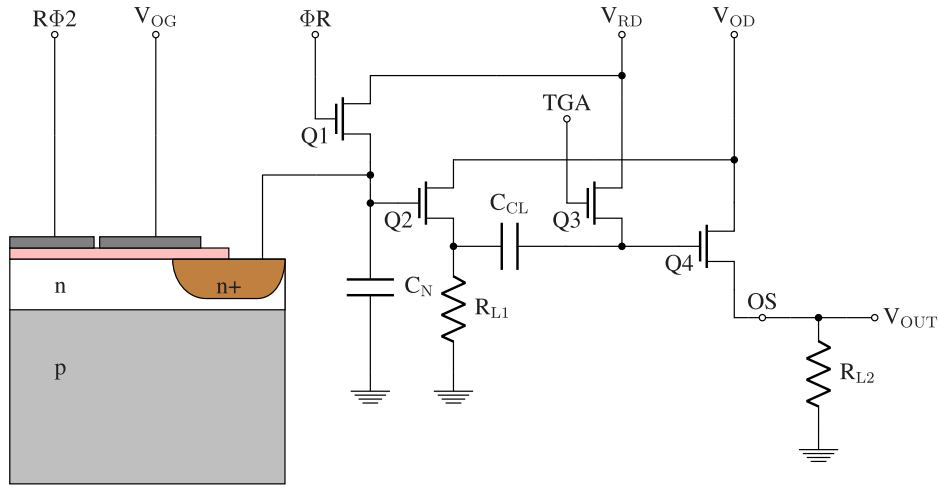


**Fig. 1** Schematic representation of a two-stage CCD output. All components shown except the second stage load  $R_{L2}$  are on-chip. The capacitor marked  $C_N$  represents the junction capacitance of the pn junction sense node.

$$\sigma_{\text{rms}}[e^-] = \frac{\sqrt{k_B T C_N}}{q_e}, \quad (2)$$

where  $q_e$  is the electronic charge. At the nominal LSST operating temperature of  $T = 203$  K and assuming a typical sense node capacitance of  $C_N = 15$  fF leads to  $\sigma_{\text{rms}}[e^-] \approx 40e^-$ . The reset noise can be effectively canceled by measuring the individual reset level for each pixel readout and subtracting the signal level from it using a CDS process. Perhaps, the most common implementation of CDS in the analog domain is the dual slope integrator (DSI), also known as the differential averager (DA), which is illustrated in Fig. 2. It is useful to refer to this diagram even in the digital correlated double sampling (DCDS) case, since the operation of the digital DA system is equivalent to this circuit in the limit of infinite sample rate. In fact, taking some simplifying assumptions, it can be shown that a DSI is a matched filter for the subtraction of pixel values in the absence of  $\frac{1}{f}$  noise.<sup>5</sup> Optimal filtering can also be designed in the presence of  $\frac{1}{f}$  noise, using either advanced digital filtering methods enabled by a DCDS system<sup>8</sup> or modified analog clamp and sample circuitry.<sup>9</sup> However, the question of selecting the best timing parameters for the circuit remains, even where the

gain and (if applicable) filter coefficients have been matched to the system noise spectrum.

A diagram of how a video signal looks before CDS processing is shown in Fig. 3. Throughout this work, we label four CDS timing parameters as follows:

- $a$  is the offset from the start of the pixel to the beginning of the reset sampling window,
- $L_a$  is the length of the reset sampling window,
- $b$  is the offset from the start of the pixel to the beginning of the signal sampling window, and
- $L_b$  is the length of the signal sampling window.

A processed pixel value is obtained by a simple procedure, described here in terms of the operation of the circuit shown in Fig. 2. The CLAMP and RESET switches are typically operated simultaneously with the reset feedthrough transient, to restore the DC level of the processor. At time  $a$ , the switch  $\text{INT}_-$  is closed, and remains so for a period  $L_a$ , during which the negative integral of the video reset window accumulates on the capacitor  $C_{\text{int}}$ . At time  $b$ , switch  $\text{INT}_+$  is closed, which causes the integral of the signal window to be added to that of the reset window. The resulting output is the pixel value. The procedure

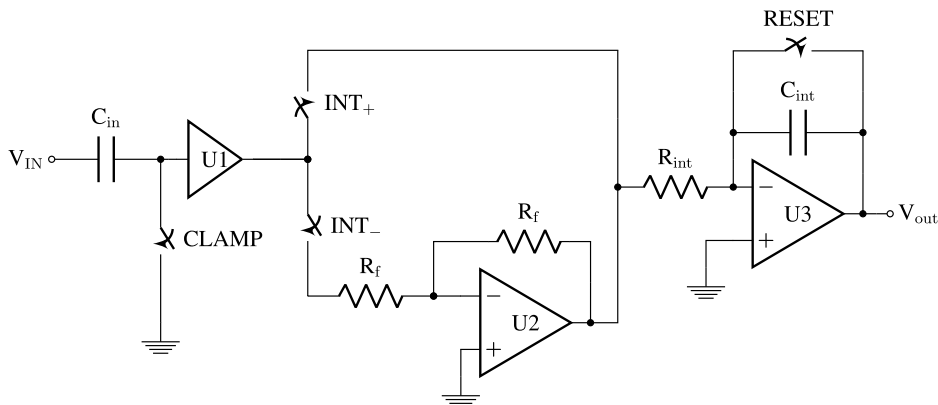


**Fig. 2** Schematic representation of a DSI circuit.

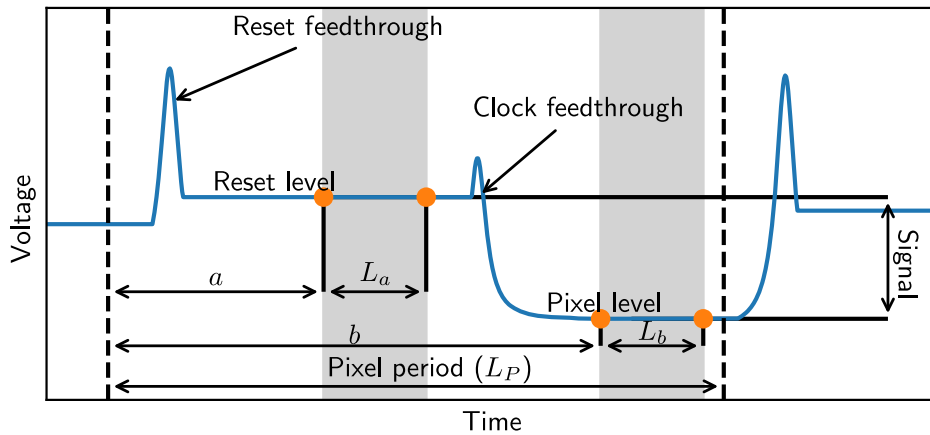


**Fig. 3** Cartoon diagram of a CCD video signal output. ( $a, b, L_a, L_b$ ) are the CDS timing parameters.  $L_P$  is the pixel period.

for DCDS is conceptually the same, except that the signal is oversampled during the sampling windows by a fast analog-to-digital converter (ADC), and the integration and subtraction are performed digitally.

### 3 Methods

The test system consists of an Teledyne-e2v CCD250 device cooled via liquid nitrogen to an operating temperature of  $-100^\circ\text{C}$ , readout using an Semiconductor Technology Associates Archon system,<sup>10</sup> and illuminated by a stabilized quartz-tungsten light source passed through a monochromator. A more detailed description of this test system has been previously published.<sup>11</sup>

The Archon readout carries 16 16-bit 100-MHz ADCs, one for each output channel of the CCD250. The CDS is performed internally to the controller, and it is not possible to apply non-unity weighting coefficients to the samples before processing. In this manner, the system quite closely approximates a DSI, even for the fairly rapid pixel rate used. It is possible to readout the raw (pre-CDS) sample values for a specified region of an image for a single channel at a time. For all the results shown here, we selected a region of  $512 \times 200$  pixels (each channel has 512 columns and 200 rows in total). This results in  $\sim 220$  MB of raw data per captured image. The timing sequence used yielded a pixel rate of 490 kHz, resulting in a pixel period  $L_P = 204$  (all CDS timing parameters are given in numbers of 100 MHz samples).

Flat-field data were captured for 8 of the 16 total channels, each consisting of 5 bias frames and 40 pairs of illuminated frames up to an integration time of 5 s. The backside bias of the CCD was set to  $V_B = -60$  V, and in future, it would be of interest to study the effect of changing bias voltages (the backside bias used significantly alters readout conditions, including the capacitance of the sense node<sup>12</sup>). Using the raw sample data, we can then *post facto* reconstruct a photon transfer curve (PTC) for a set of CDS timing parameters in software using exactly the same underlying readout data. This process is very simple and consists of summing and normalizing the sample values in an identical manner to the DA in the Archon firmware. We verified for two randomly selected sets of parameters that our reconstructed pixel values were identical to the Archon pixel values with CDS enabled. We construct the PTC following the standard procedure, including subtraction of a mean overscan value for each row, subtraction of a bias frame before calculation of mean

value, and differencing of two illuminated images to eliminate fixed pattern noise before calculating variance.<sup>13</sup>

### 4 Effect of Correlated Double Sampling Timing on Linearity and Noise

It is clear that the values of  $L_a$  and  $L_b$  significantly affect the SNR of the image. Intuitively, longer sampling times suppress the white noise component. This is found to be the case in practice. The values of  $a$  and  $b$  also affect SNR because sampling near the region of a clock edge transition (which injects noise) increases the total integrated noise. This second effect is illustrated in Fig. 4(b) where the change of  $(a, b) = (50, 105)$  to  $(a, b) = (85, 110)$  significantly increases the measured noise floor  $\sigma$ .

We also calculate the linearity residuals (LRs)  $\alpha$  for the data according to the equation from Janesick:<sup>3</sup>

$$\alpha_i = 100 \times \left( 1 - \frac{S_{\text{mid}} t_i}{S_i t_{\text{mid}}} \right), \quad (3)$$

where  $S_i$  and  $t_i$  are the mean signal levels and integration times, respectively; and  $S_{\text{mid}}$  and  $t_{\text{mid}}$  are the mean signal level and integration time at a selected midpoint, respectively. In this work, we use  $t_{\text{mid}} = 2.5$  s. Again, it is intuitive that having sampling periods which either overlap a clock feedthrough or are too early after the decay of the reset transient will incur significant linearity errors, since the magnitudes of these transients do not depend linearly on the sense node charge. In Fig. 4, we see this in action. We start from a very poor linearity situation ( $|\alpha_i|_{\text{max}} > 2\%$ ) with  $(a, b) = (50, 120)$  and dramatically improve by making the signal sampling period later with  $(a, b) = (50, 135)$ . We expect, however, that  $L_a$  and  $L_b$  should have weak effect on linearity by themselves, though too large a choice for these parameters would force the sampling periods into problematic regions. Thus, the set of timing parameters which optimize SNR is almost always not the same as that which optimizes LR, and that these two goals are in contention. It is also conceivable that a different set of timing parameters would optimize linearity and SNR over some signal ranges than others.

### 5 Optimizing Correlated Double Sampling Parameters

Strictly, the optimization problem presented to us is one of mixed-integer programming (since the timing values are restricted to be integers), which is well-known to be NP-hard.

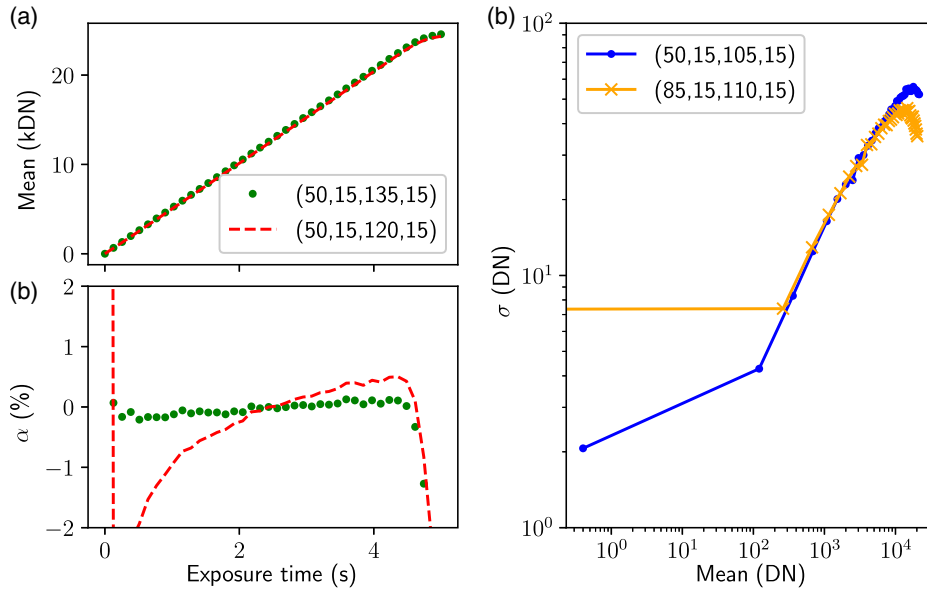


**Fig. 4** Examples of (a, c) linearity and (b) PTC curves for different CDS timing values. The timing parameters are given as  $(a, L_a, b, L_b)$ .

However, through analogy to an analog CDS system where the timing parameter values are continuous, we expect that where it is possible to select noninteger sample numbers, all the resulting cost functions should be well defined and smooth. Hence, it is suitable to use standard Nelder–Mead multivariate optimization routines (as implemented in the SciPy package),<sup>14</sup> and to calculate the cost functions for noninteger values by linearly interpolating from the nearest integer value results. As mentioned in Sec. 4, it is likely that for some applications (e.g., low light imaging) one might tailor a cost function to optimize CDS timing in some specified signal range, or to emphasize linearity and SNR to different degrees. In this work, we consider the optimization over the following cost functions:

$$f_{\text{SNR}} = \frac{\langle S \rangle_{\text{pix}}}{\sigma_{\text{bias}}}, \quad (4)$$

$$f_{\text{lin}} = \sqrt{\langle \alpha^2 \rangle}, \quad (5)$$

$$f_{\text{comb}} = \frac{f_{\text{SNR}}}{f_{\text{lin}}}, \quad (6)$$

where  $\langle x \rangle$  indicates taking a mean average. Several more natural cases worthy of investigation would be the maximum LR (as opposed to the rms value represented by  $f_{\text{lin}}$ ), and combining SNR and linearity with different powers in  $f_{\text{comb}}$ , which are not considered further here.

Two cross sections for  $f_{\text{SNR}}$  in  $(a, b)$  and  $(L_a, L_b)$  are shown in Fig. 5. These give a somewhat intuitive picture, with a longer and later reset period  $L_a$  clearly improving SNR to avoid the reset transient. The resulting parameters from the full four-dimensional maximization are shown in Fig. 8(a). The optimized parameters appear to contain significant parts of the clock feedthrough region, which will clearly be detrimental to linearity performance.

Next the minimization of  $f_{\text{lin}}$  is considered. Cross sections in  $(a, b)$  for two different  $L = L_a = L_b$  values are shown in Fig. 6. We see that positioning either of the sampling windows in

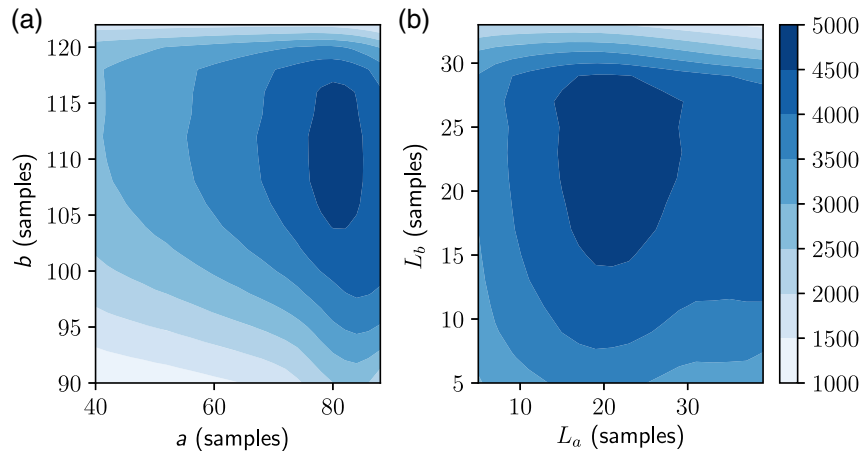


**Fig. 5** (a) Cross sections for  $f_{\text{SNR}}$  through  $(a, b)$  at constant  $L_a = L_b = 20$  and (b) through  $(L_a, L_b)$  at  $(a, b) = (80, 110)$ .

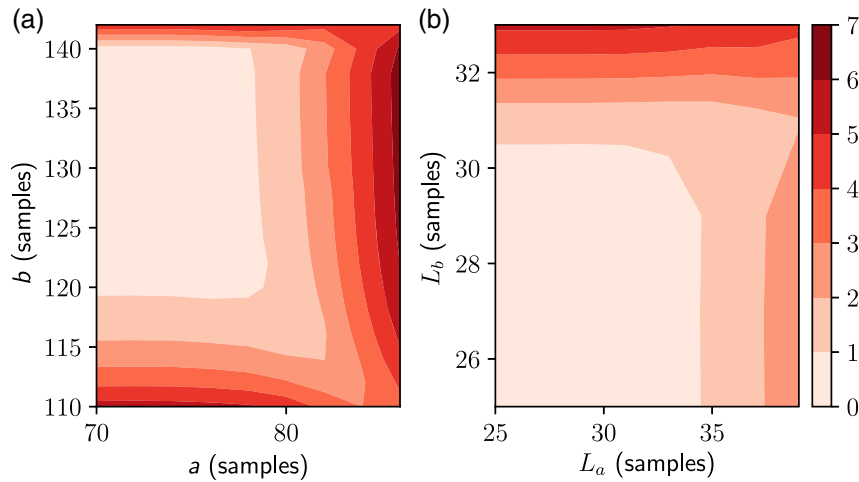


**Fig. 6** (a) Cross sections for  $f_{\text{lin}}$  through  $(a, b)$  at constant  $L_a = L_b = 20$  and (b) through  $(L_a, L_b)$  at  $(a, b) = (75, 130)$ .

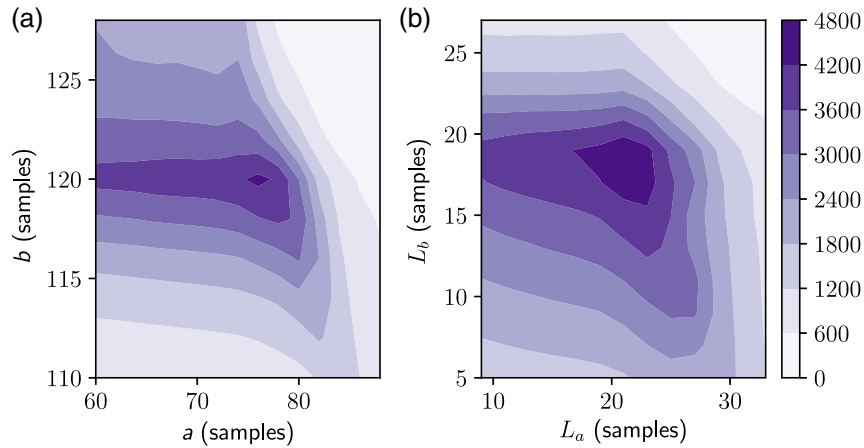


**Fig. 7** (a) Cross sections for  $f_{\text{comb}}$  through  $(a, b)$  at constant  $L_a = L_b = 20$  and (b) through  $(L_a, L_b)$  at  $(a, b) = (75, 120)$ .

regions of rapid clock transitions decreases linearity as expected. Placing the reset region as late as possible consistent with not crossing into the serial clock feedthrough is also seen to be optimal. However, the resulting parameters in Fig. 8(b) are somewhat confusing. It appears that the optimized signal window is placed very “late”—well into the region where the video has

stopped being flat after transferring signal charge. We will discuss a possible reason for this counter-intuitive result in Sec. 6.

Finally, we show the results of a combined optimization. Cross sections are shown in Fig. 7, and the optimized parameters in Fig. 8(c). The chosen parameters clearly represent a compromise between the considerations of SNR and linearity, though

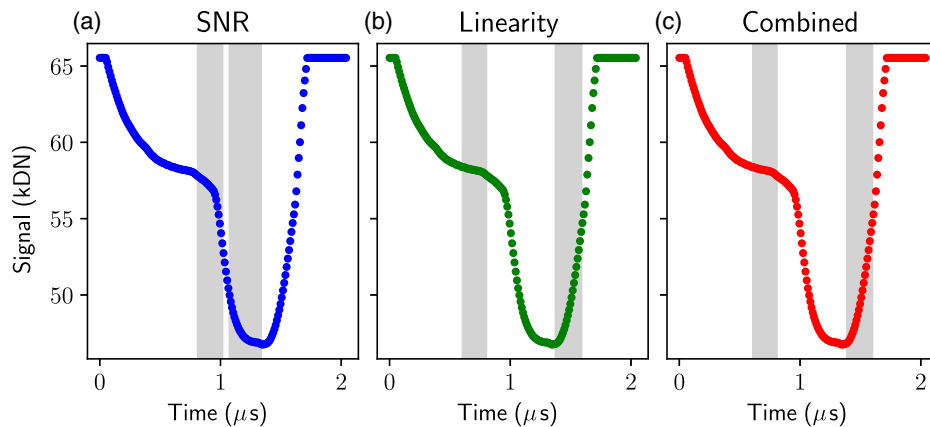


**Fig. 8** Optimum CDS timing parameters (gray shaded) and corresponding raw pixel sample values, optimizing for (a) signal to noise ratio, (b) linearity, and (c) SNR/linearity



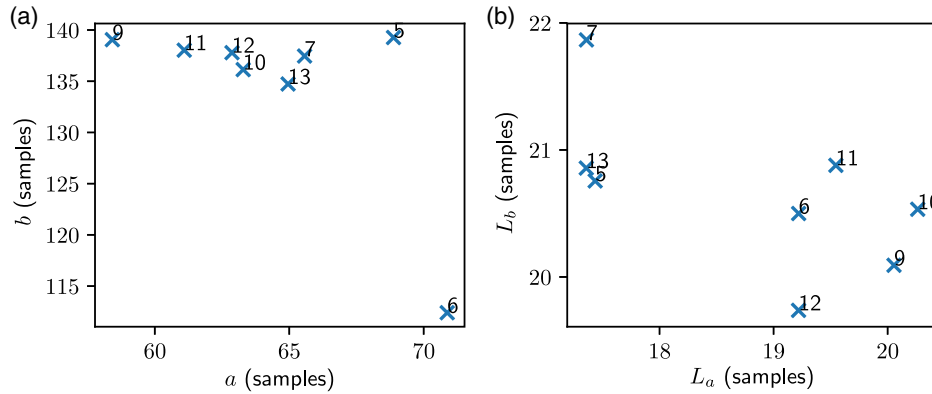


**Fig. 9** Combined optimized timing parameters for different CCD channels. Each point is labeled with its channel index. Left panel: cut through  $(a, b)$  space. Right panel: cut through  $(L_a, L_b)$  space.

the signal sampling window is found to be later than might be selected by the eye.

In Fig. 9, the parameters resulting from combined optimization for all eight channels measured are shown. A reasonably tight grouping both in terms of sample window position (except for the outlier channel 6) and window length are exhibited. It seems reasonable that selecting parameter values in some centroid of the located points for various channels would be a suitable compromise to optimize the entire device readout (though a higher-dimensional procedure which separately took into account the data for all channels simultaneously could be contemplated).

## 6 Subtraction of Raw Video Signals

Consider the operation of a DA, which takes a set of raw ADC samples  $\hat{x}_n$  and turns them into a pixel value  $X_j$  with timing parameters  $(a, b, L_a, L_b)$ :

$$X_j = \frac{1}{L_a} \sum_{n=a}^{a+L_a} (\hat{x}_n) - \frac{1}{L_b} \sum_{i=b}^{b+L_b} (\hat{x}_n). \quad (7)$$

In a scientific context, one almost universally wishes to subtract two pixel values to yield a final pixel value (e.g., subtracting a bias frame pixel value  $Y_j$  from the corresponding image frame value  $X_j$ ). Consider the output of our DA in such an operation:

$$X_j - Y_j = \left[ \frac{1}{L_a} \sum_{n=a}^{a+L_a} (\hat{x}_n) - \frac{1}{L_b} \sum_{i=b}^{b+L_b} (\hat{x}_n) \right] - \left[ \frac{1}{L_a} \sum_{n=a}^{a+L_a} (\hat{y}_n) - \frac{1}{L_b} \sum_{i=b}^{b+L_b} (\hat{y}_n) \right]. \quad (8)$$

If we can assume that the low-frequency noise component and DC offset drift are small (and thus the difference between the raw samples  $x_n$  and  $y_n$  is constituted by the response of the system to different pixel values), then the linearity of the DA operation implies we could rearrange Eq. (8) to give

$$X_j - Y_j = \frac{1}{L_a} \sum_{n=a}^{a+L_a} (\hat{x}_n - \hat{y}_n) - \frac{1}{L_b} \sum_{n=b}^{b+L_b} (\hat{x}_n - \hat{y}_n) \quad (9)$$

or, in other words, there is in principle no reason why we could not subtract the raw video for two pixel values sample by sample

rather than subtracting the pixel values after CDS processing. Such an operation is of very little practical use, since in reality the low-frequency noise component may be significant. In addition, for acquisition of a whole image frame this method would require an excessive (and unnecessary) data volume. However, this operation does provide some insight (at least in the specific system readout discussed in this work) into why the optimized values of  $a$  and  $b$  seem to be found later than would be intuited by “eyeballing” the raw samples. We show the results of this operation for two randomly selected pixels in Fig. 10. It is much clearer here how the optimized values of  $a$  and  $b$  might be arrived at through the procedure described in Sec. 5—since the rising edges at the end of the signal region are very similar between the image and bias pixels, their subtraction results in the appearance of a much longer “flat” portion of the pixel signal than we see in the nonsubtracted traces.

We do not wish to make the claim that this effect applies to all readout systems—it is likely that when  $\frac{1}{f}$  noise is significant, or there is large jitter in clock timings and thus inconsistent clock feedthrough positions through time, then the raw subtraction method may well not give good insights into optimization. However, in situations where these limitations do not apply, this operation provides excellent insight into choosing CDS timing values.

The raw sample subtraction method is especially intriguing in the context where a DCDS system is not available—the linearity property of the DA operation applies equally to that of an analog circuit such as a DSI. Thus, only a few traces of pre-CDS video data (obtained e.g., from an oscilloscope) would be needed to get a much clearer picture for timing optimization.

The procedure using an analog CDS system would be roughly as follows.

1. Use the CCD timing generator to produce a trigger pulse at some chosen pixel within the image readout.
2. Use an external data acquisition system (e.g., an oscilloscope) to capture the raw video trace of this pixel before CDS processing.
3. Vary the integration time (and thus signal level) and repeat this capturing process.
4. Numerically construct raw subtracted traces for each integration time and determine values of  $a$  and  $b$  for which linearity performance appears acceptable.

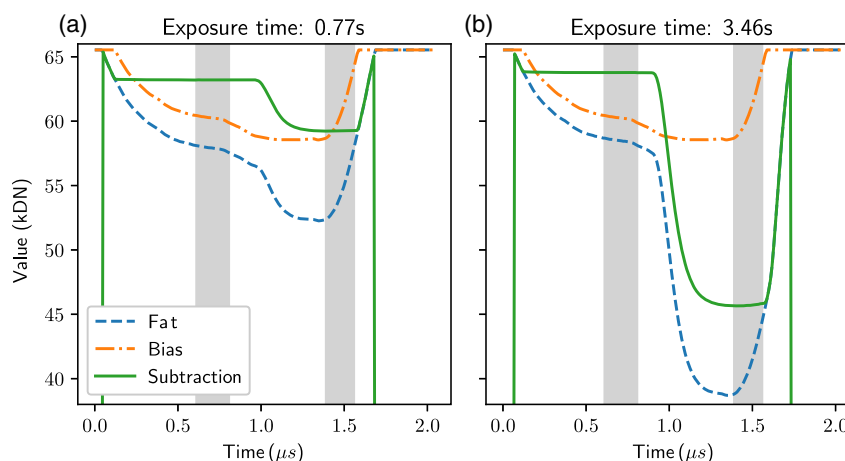


**Fig. 10** Subtracting the raw samples of a bias pixel from an image pixel for two different exposure times. The shaded vertical regions show the optimized CDS values obtained previously. (a) Exposure time of 0.77s. (b) Exposure time of 3.46s.

5. Using these  $a$  and  $b$  values, vary  $L_a$  and  $L_b$ , reading out whole images from the system for each value, and measure the SNR to find the maximum values consistent with the required SNR.

Unfortunately, no readout system equipped with analog CDS was available for this work. However, we hope to test this optimization procedure in future to determine its efficacy in a real-world situation.

## 7 Conclusions

The effect of changing only the CDS timing parameters with all other operating conditions of a CCD held constant has been investigated using raw sample capture from a DCDS readout. We have shown that numerical optimization is a viable way to choose parameters which optimize a trade-off between SNR and linearity.

The observed optimal values in our particular system were observed to be counter-intuitive in the sense that they appear in a region where the raw signal is rapidly changing rather than stable. We have developed an explanation for this by considering the raw sample by sample subtraction of two pixel values, which shows that after processing, these regions remain flat and suitable for use in CDS integration periods. No applicability of this effect is assumed for all readout systems, though the insight from the subtraction method is likely to be useful in many wider contexts than considered in this work.

It is recommended that in CDS optimization of a CCD readout, the subtraction of two raw video signals should be included as part of the inputs to choosing the timing parameters.

## Acknowledgments

This work has been partially supported by Science and Technology Facilities Council funding for UK participation in LSST, through Grant ST/N002547/1. The authors wish to acknowledge also useful conversations with Chris Damerell of Oxford University.

## References

1. V. Radeka et al., “LSST sensor requirements and characterization of the prototype LSST CCDs,” *J. Instrum.* **4**(3), P03002 (2009).
2. Z. Ivezić et al., “LSST: from science drivers to reference design and anticipated data products,” *Astrophys. J.* **873**(1), 111 (2019).
3. J. R. Janesick, *Scientific Charge-Coupled Devices*, SPIE Press, Bellingham, Washington (2001).
4. G. Hopkinson and D. Lumb, “Noise reduction techniques for CCD image sensors,” *J. Phys. E Sci. Instrum.* **15**(11), 1214–1222 (1982).
5. K. D. Stefanov, “Digital CDS for image sensors with dominant white and 1/f noise,” *J. Instrum.* **10**, P04003 (2015).
6. P. R. Jorden et al., “e2v new CCD and CMOS technology developments for astronomical sensors,” *Proc. SPIE* **9154**, 91540M (2014).
7. H. Nyquist, “Thermal agitation of electric charge in conductors,” *Phys. Rev.* **32**, 110–113 (1928).
8. J. Gach et al., “A new digital CCD readout technique for ultra-low-noise CCDs,” *Publ. Astron. Soc. Pac.* **115**(811), 1068–1071 (2003).
9. H. M. Wey and W. Guggenbuhl, “An improved correlated double sampling circuit for low noise charge coupled devices,” *IEEE Trans. Circuits Syst.* **37**, 1559–1565 (1990).
10. G. Bredthauer, “Archon: a modern controller for high performance astronomical CCDs,” *Proc. SPIE* **9147**, 91475B (2014).
11. D. Weatherill et al., “An electro-optical test system for optimising operating conditions of CCD sensors for LSST,” *J. Instrum.* **12**, C12019 (2017).
12. M. S. Robbins, P. Mistry, and P. R. Jorden, “Detailed characterisation of a new large area CCD manufactured on high resistivity silicon,” *Proc. SPIE* **7875**, 787507 (2011).
13. J. R. Janesick, *DN to  $\lambda$* , Press Monographs, SPIE Press, Bellingham, Washington (2007).
14. T. E. Oliphant, “Python for scientific computing,” *Comput. Sci. Eng.* **9**, 10–20 (2007).

**Daniel P. Weatherill** is a postdoctoral researcher at the University of Oxford. He earned his bachelor’s and master’s degrees in experimental and theoretical physics from the University of Cambridge, and a PhD in spaceflight instrumentation from the Open University. His current work mainly focuses on testing, modeling, and optimizing the operation of CCD detectors for the LSST telescope.

**Ian Shipsey** is a principal investigator (PI) of LSST-UK CCD characterization. He is Henry Moseley professor of physics at Oxford University, and a co-I of the Mu3e tracker and ATLAS HL-LHC pixel detector. He was co-PI of the CMS at LHC phase-0 forward pixel detector (2008) and PI of the CLEO-III Silicon Vertex Detector (2000). He received the 2019 James Chadwick Medal and prize of the UK Institute of Physics for elucidation of the physics of heavy quarks.

**Kirk Arndt** is a silicon development engineer. He is lead engineer for the module assembly of the ATLAS HL-LHC pixel detector, and Mu3e tracker. Previously he played a leading role in the silicon vertex detectors for CLEO II.V (1995), the CLEO III (2000), and the CMS



Phase 0 (2008) and Phase 1 (2014) Silicon Forward Pixel Detectors, and in the design of the camera for the Large Synoptic Survey Telescope.

**Richard Plackett** is the lead silicon detector scientist for the OPMD cleanroom facility at Oxford University (2014). His principal interests are the upgrade for the ATLAS pixel system, the Mu3e experiment, and the Medipix collaboration. He has previously worked on hybrid pixel detector development for Diamond Light Source (2011), was a CERN fellow with the microelectronics group (2008), and worked at Imperial College on the LHCb RICH hybrid pixel photon detector system (2002).

**Daniel Wood** is a postdoctoral researcher within the OPMD group at the University of Oxford, working on silicon detector development. Prior to joining the group, he completed a PhD in radiation damage studies from the Centre for Electronic Imaging at the Open University.

**Kaloyan Metodiev** is a doctoral student at the University of Oxford, Particle Physics Department, working in the Oxford Physics Microstructure Detector (OPMD) Laboratory. He completed his bachelor's and master's degrees at Trinity College, University of Oxford. As part of OPMD, his main research interests lie in silicon detector devices,

and he is actively involved in the laboratory's work and associated projects.

**Maria Mironova** received her BSc degree in physics from the University of Goettingen, Germany, and an MSc degree from Imperial College London. She is now pursuing a PhD in detector development at the University of Oxford.

**Daniela Bortoletto** is a professor of particle physics and the head of particle physics at the University of Oxford. She is a member of the ATLAS at CERN and the Mu3e collaborations at PSI. Her main research interests are Higgs physics and the development of hybrid and monolithic silicon detectors for hadron and  $e+e-$  colliders. For Mu3e, she is focusing on the construction of a very light pixel detector.

**Nicolas Demetriou** is a postgraduate student at Imperial College London, interested in computational physics. He earned his theoretical physics degree from the University of Glasgow, working on machine learning applications for beyond the standard model searches. His research experience also includes the investigation of birefringent materials and pressure-wave propagation in granular media at German Aerospace Center, and the optimization of CDS timing parameters at Oxford Particle Microstructure Detector Facility, under the supervision Dr. Dan Weatherill.